

# Control of a SiC 2.5 MHz resonant full-bridge inverter for inductively driven plasma

Christoph Simon<sup>1</sup>, Santiago Eizaguirre<sup>1</sup>, Fabian Denk<sup>1</sup>, Michael Heidinger<sup>1</sup>, Rainer Kling<sup>1</sup>, Wolfgang Heering<sup>1</sup>

<sup>1</sup> Karlsruhe Institute of Technology, Light Technology Institute, Germany

Corresponding author: Christoph Simon, christoph.simon@kit.edu

## Abstract

The electronic ballast of an inductively driven plasma faces a mostly inductive, variable load impedance. The SiC full-bridge inverter uses the inductive behavior to achieve zero-voltage-switching and a switching frequency of 2.5 MHz, at 3.9 kVA and 764 W in the plasma. The control is realized on a modern, small TI Piccolo microcontroller with a high-resolution PWM module and compensates for the variable load impedance. We present design and experimental results of a 2.5 MHz inverter for inductively driven plasma without the need for a large FPGA controller.

## 1 Introduction

With the current generation of SiC MOSFETs, resonant inverters for very high output frequency of 2.5 MHz are feasible. On one hand, such a high switching frequency promises efficiency gain and higher power density, but on the other hand, stress on passive components as well as the filter effort for electromagnetic compatibility increases [1]. Some applications, however, benefit greatly from a high-frequency alternating current, for example inductively driven plasmas, inductive heating or wireless charging.

In this paper, we present a resonant SiC full-bridge inverter with an output frequency of 2.5 MHz and control for an inductively coupled plasma of an UV lamp. The high-frequency current allows for an efficient inductive coupling of the power into the lamp and a very high UV efficiency of the plasma.

We used to implement the switching signal generation for our 2.5 MHz inverters on a larger FPGA in a separate control unit and transmit the signals with optical fibers [2]. While this is robust, it is also large, expensive and draws a lot of auxiliary power. But in the meantime, modern, small microcontrollers offer high-resolution PWM modules.

For this inverter, the controller software and pulse



**Fig. 1:** Image of the inductively driven lamp. The induction coil is wound around a cylindrical lamp vessel.

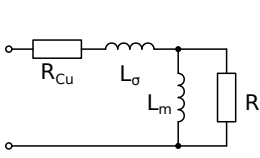
generation runs on a TI Piccolo microcontroller (Texas Instruments, USA). While this is a small microcontroller, which runs at 100 MHz, it offers a high-resolution PWM module with a resolution of 150 ps and allows fine-grained tuning of the 2.5 MHz switching signals and power control of the load.

In section 2, we will discuss the load behavior of the inductively driven plasma in detail. Sections 3 and 4 present the design of the inverter and the controller. Section 5 contains the experimental results of the inverter system while driving a plasma inductively.

## 2 Load behavior

The inductively driven plasma is inside a cylindrical lamp vessel with an induction coil wound around. Figure 1 is an image of the lamp.

The equivalent circuit of the inductively driven plasma, shown in Fig. 2 (left), is a transformer with a complex and variable load impedance. The



$N$	45
$d$	75 mm
$d_w$	1 mm
$f$	2.5 MHz
$R_{Cu}$	$2.8 \Omega$

**Fig. 2:** (left) Schematic of the equivalent circuit of the inductively driven plasma. It is a transformer, loaded with the plasma resistance  $R$ . (right)  $R_{Cu}$  calculation result of Eq. (1) and parameters of the induction coil of the UV lamp.

induction coil is the primary winding and the plasma is a one-turn secondary winding. There are very sophisticated models about the complex load impedance and detailed plasma behavior in literature [3]. However, from a power supply perspective, we model the complex and variable impedance as a variable resistor. The inductive and capacitive effects of the plasma are relatively small and are compensated by the stray inductance of the transformer model.

When the lamp is off, the resistance is infinite and the transformer is not loaded. With plasma ignition, the resistance drops suddenly to a specific value. From then on, it is temperature dependent and changes slowly over time, while the lamp heats up and reaches the steady-state temperature.

The electronic ballast shall control the lamp power and compensate for the resistance changes. It shall achieve short heat-up time and optimal efficiency during operation. Furthermore, the inductive coupling is more efficient with higher operating frequency as investigated in [4].

## 2.1 Equivalent circuit parameters

This section presents an estimation of the values of each element in the equivalent circuit in Fig. 2.

The copper resistor  $R_{Cu}$  accounts for the resistance of the long copper wire of the lamp coil. It is calculated with the conductivity of copper  $\kappa$ , the length of the wire  $l_w$  and the effective cross-section caused by the skin effect:

$$R_{Cu}(f) \approx \frac{2l_w}{d_w} \sqrt{\frac{f\mu_0}{\pi\kappa}} \quad \text{and} \quad l_w = N\pi d \quad (1)$$

The skin effect increases the wire resistance

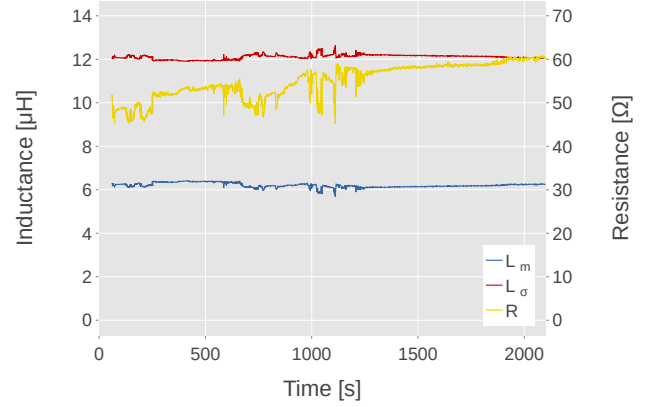


**Fig. 3:** Equivalent circuit parameters  $L_m$ ,  $L_\sigma$  and  $R$  over 30 min heat-up time at 764 W.

considerably due to the high operating frequency. The proximity effect between two adjacent wires of the winding is not taken into account because of the coarse winding. The distance between two windings of the lamp is about 22 mm. Equation (1) was also discussed and tested in the previous paper [2].

Figure 2 (right) presents the result for this lamp.  $R_{Cu}$  is  $2.8 \Omega$  and very small compared to the other impedance values in the equivalent circuit.

The remaining parameters  $L_m$ ,  $L_\sigma$  and  $R$  are calculated from voltage and current measurement at the lamp coil terminals. Details of the measurement are described in section 5, “Experimental results”.

With reduced input voltage, while the lamp is not ignited, the plasma resistance  $R$  is infinite. The lamp impedance is caused by the coil inductance  $L_{coil}$ , which is equal to the sum of  $L_m$  and  $L_\sigma$ .

The impedance of the lamp coil, while the lamp is off, is  $288 \Omega$ . At a frequency of 2.5 MHz, this equals a coil inductance  $L_{coil}$  of  $18.3 \mu\text{H}$ . Also, a measurement of the lamp coil with an 4395A impedance analyzer (Agilent, USA), results in about  $18 \mu\text{H}$ .

While the lamp is on, the coil is loaded with the plasma resistance  $R$ . The measured lamp impedance comprises  $L_m$ ,  $L_\sigma$  and  $R$ . The three parameters are calculated from the impedance magnitude, phase and the coil inductance  $L_{coil}$ .

Figure 3 shows the equivalent circuit parameters  $L_m$ ,  $L_\sigma$  and  $R$  over about 30 min runtime. The

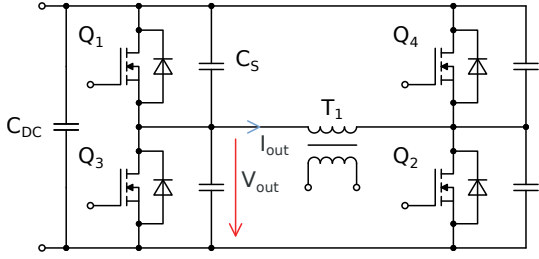


**Fig. 4:** Schematic of the full-bridge inverter. Each SiC MOSFET has a parallel snubber capacitor. The load is connected through a transformer.

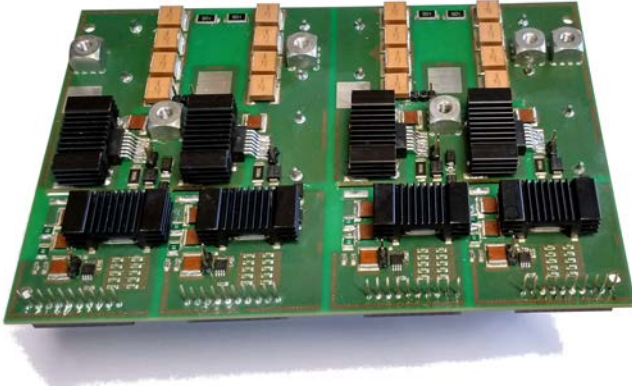


**Fig. 5:** Image of the SiC 2.5 MHz full-bridge inverter.

inductance values are mostly constant over time, but the resistance changes with the lamp temperature.

The stray inductance is  $L_\sigma = 12.1 \mu\text{H}$  and the main inductance is  $L_m = 6.2 \mu\text{H}$ . The plasma resistance (transformed to the primary side of the transformer) changes from  $50 \Omega$  after ignition to a steady-state value of  $60 \Omega$ . Depending on the state of the lamp, the resistance might go through an intermediate maximum before it settles for the steady-state value.

### 3 Inverter

The inverter of the electronic ballast is a full-bridge inverter with SiC MOSFETs C3M0065090J (Cree, USA) in the TO-263-7 (D2PAK) package. The MOSFET has a separate drive-source pin to decouple the gate driver from the power path and to allow very high slew rates at the switch node. Figure 4 shows the schematic and Fig. 5 shows an image.

The DC-Link capacitance is realized with Ceralink B58031U9254M062 (TDK, Japan) ceramic

capacitors and MKP1848C DC-Link (Vishay, USA) film capacitors.

For the SiC MOSFETs to withstand high-frequency switching at 2.5 MHz, some form of switching loss reduction is necessary, because switching losses increase linearly with the switching frequency. In the inverter, each MOSFET has a parallel snubber capacitor, which reduces some of the switching-off losses. Also, the inverter implements zero-voltage-switching (ZVS) [5].

The inverter is loaded with a transformer and a resonance circuit formed of a parallel capacitor and the lamp coil. At the operating frequency, the resonant load behaves inductively. When a MOSFET switches off, the inductive load current charges the snubber capacitor and output capacitance of this MOSFET and discharges the ones of the other MOSFET. The voltage of the switch node swings from one potential of the DC-Link to the other and the other MOSFET can switch on a little later under zero-voltage condition.

#### 3.1 Snubber

The size of the snubber capacitor can be calculated from the commutation time, the output current magnitude and phase.

The output current is:

$$I(t) = -\hat{I} \sin(\omega t - \phi), \omega = 2\pi f \quad (2)$$

with a phase shift of  $\phi$  to the trapezoidal output voltage. The current shall just be able to charge or discharge the effective output capacitance  $C_{\text{eff}}$  of the bridge leg during the commutation time  $t_\delta$ .

$$C_{\text{eff}} \cdot \hat{U} = \int_{-\frac{t_\delta}{2}}^{\frac{t_\delta}{2}} I(t) dt \quad (3)$$

$$C_{\text{eff}} = \frac{\hat{I}}{\hat{U}} \cdot \frac{\cos(\omega \frac{t_\delta}{2} - \phi) - \cos(\omega \frac{t_\delta}{2} + \phi)}{\omega} \quad (4)$$

Equation (4) is also discussed in [6].

The effective output capacitance of the bridge leg is the sum of the output capacitance  $C_{\text{oss}}$  of two MOSFETs and two snubber capacitors  $C_s$ .

$f$	2.5 MHz
$\hat{U}$	700 V
$\hat{I}$	7.5 A
$\phi$	70°
$t_\delta$	35 ns
$C_{\text{eff}}$	348 pF
$C_{\text{oss}}$	60 pF
$C_s$	114 pF

**Tab. 1:** Snubber capacitor  $C_s$  calculation result of Eq. (4) and parameters.

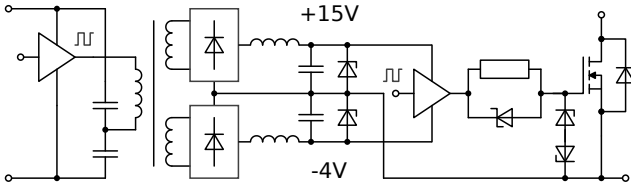


**Fig. 6:** Schematic of the gate driver. It provides two voltage levels. -4 V to switch the SiC MOSFET off reliably and 15 V to switch it on.

$$C_{\text{eff}} = 2C_{\text{oss}} + 2C_s \quad (5)$$

Table 1 shows the values for this inverter. The slew rate is defined as 20 V/ns, which equals a commutation time of 35 ns for 700 V. The calculation result for the snubber capacitor  $C_s$  is 114 pF. The inverter is equipped with 100 pF for the experiments.

### 3.2 Gate driver

The gate driver ICs are IXDN614YI (IXYS, USA). They offer high peak current and short rise times and are therefore viable for fast switching.

Each MOSFET has its own gate driver and isolated gate driver power supply unit with two voltage levels, -4 V and 15 V. The schematic of the gate driver and gate driver power supply unit is shown in Fig. 6. A



**Fig. 7:** Image of a single gate driver power supply unit.

picture of a gate driver power supply unit is shown in Fig. 7.

It is not strictly necessary to have an isolated supply unit for the two low-side MOSFETs, but the stability and robustness of the circuit benefits from the decoupling of the noise from the switching node. Also the inverter may then use the same power supply unit four times.

The isolated gate driver supply units are push-pull-converters in a half-bridge configuration. The input voltage is 21 V and the switching frequency is 80 kHz. The transformer has one primary and two secondary windings (9:4:13), one for -4 V and one for 15 V. The output of both secondary windings are rectified with diode bridge rectifiers, filtered and buffered with DC-Link capacitors. A LDO generates 3.3 V additionally for the gate signal processing ICs on the secondary side.

The supply unit does not control the output voltage or current. It is designed to reach the nominal voltages under load conditions of about 10 W. Under no load, the voltages are limited with Zener diodes to -4 V and 18 V. The positive voltage may reach higher values, because the SiC MOSFETs of the inverter are not switched on statically, so they do not see the no-load positive voltage.

The three-windings transformer is built with a toroidal core and single layer windings, which are separated over the perimeter. It achieves a low coupling capacitance from secondary to primary side. Also, with no feedback path for control from secondary to primary side, the capacitive coupling is kept small. A measurement of the supply unit with an 4395A impedance analyzer (Agilent, USA) shows a coupling capacitance smaller than 10 pF.

### 3.3 Transformer

The output transformer has 8:16 windings on two toroidal iron powder cores. The core material is Material Mix 2 (Micrometals, USA) and the size is T400-2D. The windings are single-layer and separated over the perimeter of the cores, to minimize the coupling capacitance and prevent the switching noise from propagating. The wire is a solid copper wire with 2 mm diameter.

## 4 Controller

The controller generates the high-frequency and high-resolution gate signals for the SiC MOSFETs of the full-bridge inverter. With a high resolution, the controller is able to control the output power and to adjust it in small steps.

The load of the inverter is a resonance circuit formed of the inductance of the lamp coil, the stray inductance of the transformer and a parallel capacitor. The inverter operates the load at an operating point above the main resonance frequency in an inductive region of the impedance spectrum. In the inductive region, the impedance increases with 20 dB per decade. At an operating point  $f_0$  and the power  $P_0$ , a small change of the period of the gate signal  $\Delta t$  causes an output power change  $\Delta P$ :

$$\Delta P = -\Delta t f_0 P_0 \quad (6)$$

Equation (6) is valid for an operating point away from the resonance frequency. Close to the resonance frequency, the impedance and power increase or decrease is much larger.

At an operating point of  $f_0 = 2.5$  MHz and  $P_0 = 1$  kW, for a power change of  $\Delta P = 500$  mW in a single step, the controller requires a PWM resolution for the gate signals of  $\Delta t = 200$  ps.

### 4.1 FPGA

A previous version of the inverter in [2] used an FPGA to generate the gate signals in a separate control unit and transmit them with optical fibers. While an FPGA is well suited for a fast and real time control algorithm, its clock frequency is too low for a high PWM resolution. With a clock of 40 MHz and double data rate output,  $\Delta t$  is 25 ns for a single step and the power change  $\Delta P$  is 62.5 W, which is too large for power control of a 1 kW system.

To overcome the problem of the small PWM resolution, the FPGA controller uses dithering. For some steps of 16 cycles, it sets the higher value and then for the remaining steps the lower value of the signal period, effectively subdividing the step size by 16. With dithering,  $\Delta P$  is 3.9 W effectively, which is fine enough for lamp power control.

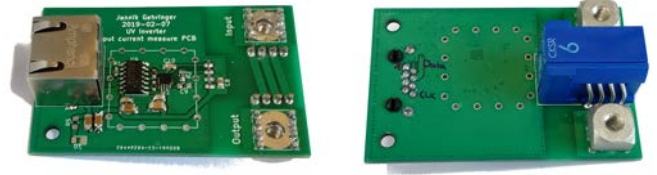


Fig. 8: Image of the input current measurement unit.

### 4.2 Microcontroller

With recent development for microcontrollers, some small microcontrollers for control applications offer high-resolution PWM modules and achieve a much higher PWM resolution, than their clock rate suggests. This inverter uses the TI Piccolo microcontroller (TMS320F280049C) (Texas Instruments, USA) with a PWM resolution of 150 ps. With Eq. (6),  $\Delta P$  is 375 mW for a single step change, which is very good for fine-grained power control.

The high-resolution PWM module supports directly the generation of a PWM signal for a bridge leg with a deadband between switching off one and switching on the other MOSFET. The frequency, duty cycle and deadband may all be set with the high resolution.

### 4.3 Signal transmission

The output pins of the high-resolution PWM module of the microcontroller are single ended. Close by the pin, a LVDS driver IC converts the gate signal to a low voltage differential signal, which has a higher immunity to electromagnetic interference.

Each signal is isolated with the digital isolator ADN4651 (Analog Devices, USA). It offers LVDS inputs and outputs, a high blocking voltage and high common-mode transient immunity of 25 V/ns at the minimum.

### 4.4 Input current measurement

The controller measures the direct input current of the inverter with a current transducer CKSR 6-NP (LEM, Switzerland). With the constant and known DC-Link voltage, it can calculate the input power. Figure 8 shows an image of the current measurement board.

The current transducer provides an analog voltage signal proportional to the current amplitude. It

is converted to a 1 bit stream with a voltage to frequency converter AD7740 (Analog Devices, USA). The digital signal is then transmitted as low voltage differential signal (LVDS) back to the microcontroller. The LVDS transmission is less susceptible to the high frequency switching noise of the inverter, than the analog voltage.

The microcontroller provides the clock to the analog to digital converter and decodes the bit stream on the “control law accelerator” (CLA) co-processor in software.

#### 4.5 Power control

The inverter operates the load in an inductive region of its impedance spectrum with rising impedance over frequency. With a fixed input voltage of the inverter, the controller can tune the switching frequency to adjust the load power.

Upon ignition, the impedance jumps to a smaller value and the power is too high. The power control may leave the settings for a while to accelerate the heat up.

The power control is implemented with an integrator. The input is the negative difference from the set power level, the output is the switching frequency. The algorithm does not need to adjust the duty cycle. The commutation time is more or less constant over a wide power range and the frequency only changes in a small interval around the nominal frequency.

To keep the power constant during lamp operation, the controller does not need to be fast. The lamp heats up in about 30 min to 1 h depending on the environment and changes only very slowly after that. Additionally, the controller will not be fast enough to compensate for ignition or capacitive load. In case of sudden capacitive load, the inverter is destroyed within microseconds. This might be enough time for emergency stop, but not for control.

### 5 Experimental results

Figure 9 shows a schematic of the experimental setup. The DC-Link is supplied by a laboratory DC power supply EA-PS 81000-30 (EA Elektro-Automatik, Germany) with limits set to 800 V and 1.3 A. During the experiment, the DC PSU operates

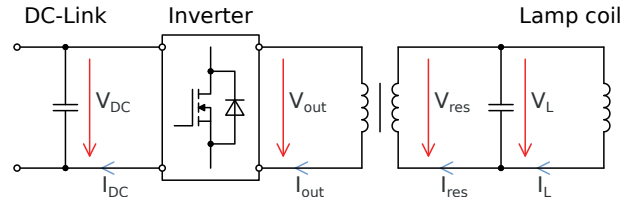


**Fig. 9:** Schematic of the experimental setup and location of the probes.

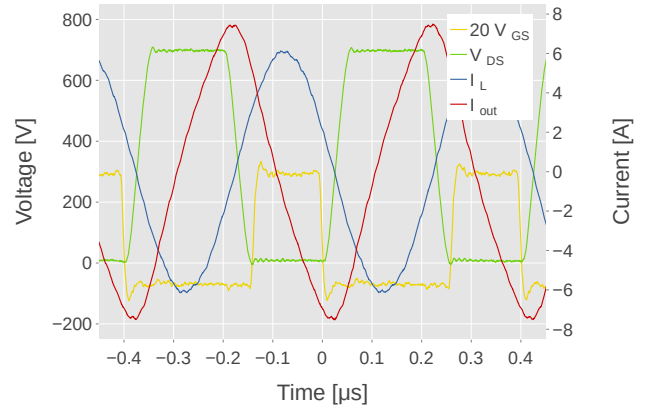


**Fig. 10:** Switching waveform.  $V_{GS}$  and  $V_{DS}$  of a low-side SiC MOSFET,  $I_L$  and  $I_{out}$ .  $V_{GS}$  is multiplied by 20 for better visibility.

at the current limit with reduced voltage around 710 V.

Another small laboratory DC power supply unit KA3005D (Korad, China) provides the 21 V auxiliary power for the controller and the gate drivers.

The experiment is observed with an oscilloscope DSOS104A (Keysight Technologies, USA). The voltage probes are BumbleBee differential voltage probes (PMK, Germany) and the current probes are current transformers 0.1 V/A (Bergoz Instrumentation, France), (Pearson, USA). The probes for the impedance measurement were carefully deskewed to each other with a 701936 deskew correction signal source (Yokogawa, Japan). Additionally, we adjusted the phase angle, so that it is  $90^\circ$  at the beginning of each measurement, when the lamp is off and the impedance is caused by the coil inductance only.

#### 5.1 Switching waveform

Figure 10 shows the switching waveform of the inverter at 2.5 MHz and about 4.1 kVA apparent power. The gate signal  $V_{GS}$  only rises, just after the

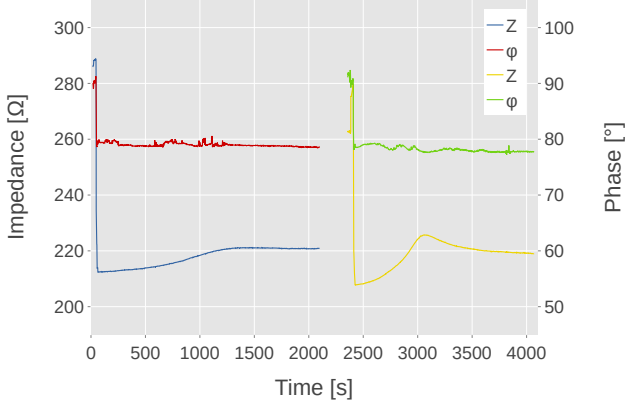


**Fig. 11:** Lamp impedance over time of two runs for about 30 min runtime each. The steady-state value is about  $220 \Omega$  and  $79^\circ$ .

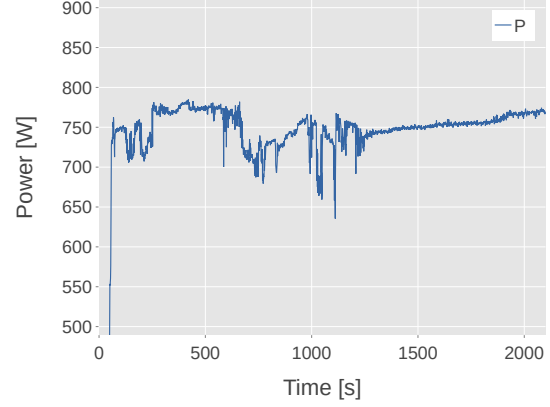


**Fig. 12:** Power over 30 min runtime. The steady-state value is about 764 W.

drain-source voltage  $V_{DS}$  reaches zero. The inverter operates with zero-voltage-switching (ZVS).

The output current  $I_{out}$  amplitude is 7.5 A and the phase shift to the trapezoidal output voltage  $V_{DS}$  is  $70^\circ$ . The rise and fall times of the voltage are 34 ns. With an amplitude of 700 V, the slew rate is about 21 V/ns. This matches very well with the design of the snubber capacitor with Eq. (4) in table 1.

## 5.2 Lamp

Figure 11 shows the impedance of the lamp over time of two runs for about 30 min runtime each.

$$Z_L = \frac{V_L}{I_L} \cdot e^{j\phi} \quad (7)$$

For both runs, the measurement starts just before the ignition of the plasma in the lamp. At ignition, the impedance jumps down to a smaller value. During lamp heat up, the impedance increases again and settles at a steady-state value. Depending on the state of the lamp, the impedance might go through an intermediate maximum during heat up.

Figure 12 shows the active power of the lamp  $P_L$ :

$$P_L = V_L \cdot I_L \cdot \cos(\phi) \quad (8)$$

The power is proportional to the lamp resistance, because the inverter is supplied by a constant current source. After heat up, the power reaches a stable value of about 764 W. The power supply values in that operating point are listed in table 2.

$P_{DC}$	941 W
$P_{AUX}$	21.0 W
$P_L$	764 W
$S_L$	3.9 kVA
$\eta$	79%

**Tab. 2:** Input power, lamp power and efficiency of the inverter driving an inductive UV lamp.

The phase angle has a very high measurement uncertainty because of the high operating frequency. Also, the active power reacts very sensitive to deviations in the phase angle, because the derivative of the cosine is high around  $80^\circ$ . Therewith, the efficiency of 79% is a rough estimation only.

The inverter achieves stable operation of the lamp at 764 W with an efficiency of 79%. The efficiency is not optimal, yet, and the apparent power of the lamp is very high with 3.9 kVA. However, lamp and resonance circuit were not optimized compared to the system of the previous paper [2], but the efficiency increased from 65% of the previous system to 79% of this system.

Figure 13 shows the output frequency of an older version of the inverter with power control enabled. By tuning the frequency, the controller was able to keep the power constant during heat up of the lamp. The frequency value is noisy, because this is the FPGA controller, which uses dithering to achieve fine control of the frequency value and power level.

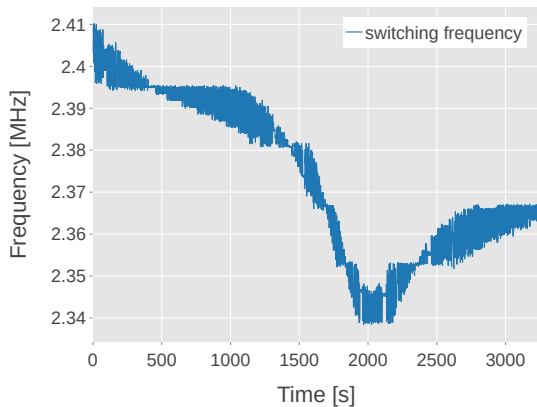


**Fig. 13:** Frequency over 1 h runtime. The measurement is noisy, because this is the FPGA controller, which uses dithering.

## 6 Conclusion

A SiC 2.5 MHz resonant full-bridge inverter for inductively driven plasma is presented. The inverter drives a 764 W, 3.9 kVA inductively coupled UV lamp and achieves an efficiency of 79% from DC-Link to the plasma, including the auxiliary power for the controller and gate drivers. The switching waveforms show zero-voltage-switching (ZVS) and a slew rate of 20 V/ns at the switch node.

The control of the inverter and inductively coupled UV lamp is implemented in software on a modern, small microcontroller with a high-resolution pulse width modulation (PWM) module. With a resolution of 150 ps, the PWM signal is fast enough for 2.5 MHz output frequency and the adjustment steps are small enough ( $\Delta P = 375$  mW), for fine grained power control of the inductively driven plasma.

The load behavior of the inductively coupled UV lamp is well modeled with an equivalent circuit of a loaded transformer. The coil around the lamp is the primary winding, the plasma forms a single-turn secondary winding. While the lamp is off, the secondary winding is an open circuit. While the lamp is on, the plasma is modeled as a variable load resistor at the secondary winding. The resistance changes in the range from  $50\ \Omega$  to  $60\ \Omega$  during 30 min heat-up of the lamp.

With the current generation of SiC MOSFETs and modern, small microcontrollers with high-resolution PWM modules, resonant inverters for very high output frequency of 2.5 MHz become affordable.

## Acknowledgment

The work is partly funded by the European Commission as part of the Horizon 2020 project “Eco-UV” under the Grant Agreement Number 641702.

Many thanks to Jannik Gehringer for the microcontroller software.

## References

- [1] J. Biela, M. Schweizer, S. Waffler, and J. W. Kolar, “SiC versus Si—Evaluation of Potentials for Performance Improvement of Inverter and DC–DC Converter Systems by SiC Power Semiconductors”, *IEEE Trans. Ind. Electron.*, vol. 58, no. 7, pp. 2872–2882, 2011. DOI: 10.1109/TIE.2010.2072896.
- [2] C. Simon, S. Eizaguirre, F. Denk, M. Heidinger, R. Kling, and W. Heering, “SiC 2.5 MHz Switching Mode Resonant Halfbridge Inverter”, in *PCIM Europe*, 2018, pp. 1–8.
- [3] E. Statnic and V. Tanach, “Investigation of the electrical discharge parameters in electrodeless inductive lamps with a re-entrant coupler and magnetic core”, *In Plasma Sources Science and Technology*, vol. 15, no. 3, p. 465, 2006.
- [4] O. Popov and J. Maya, “Characteristics of electrodeless ferrite-free fluorescent lamp operated at frequencies of 1–15 MHz”, *In Plasma Sources Sci. Technol.*, vol. 9, no. 2, pp. 227–237, 2000. DOI: 10.1088/0963-0252/9/2/317.
- [5] M. K. Kazimierczuk and D. Czarkowski, *Resonant power converters*, 2nd ed. Wiley, 2011.
- [6] K. Hähre, “Effiziente MHz-Wechselrichter mit unipolaren SiC-Transistoren für Hochleistungs-Induktionslampen”, German, PhD thesis, Karlsruher Institut für Technologie (KIT), 2016, 231 pp. DOI: 10.5445/KSP/1000055999.

## Repository KITopen

Dies ist ein Postprint/begutachtetes Manuskript.

Empfohlene Zitierung:

Simon, C.; Eizaguirre, S.; Denk, F.; Heidinger, M.; Kling, R.; Heering, W.  
[Control of a SiC 2.5 MHz resonant full-bridge inverter for inductively driven plasma](#)  
2019. PCIM Europe 2019; International Exhibition and Conference for Power Electronics,  
Intelligent Motion, Renewable Energy and Energy Management, 1753–1760, VDE Verlag  
[doi:10.5445/IR/1000144776](https://doi.org/10.5445/IR/1000144776)

Zitierung der Originalveröffentlichung:

Simon, C.; Eizaguirre, S.; Denk, F.; Heidinger, M.; Kling, R.; Heering, W.  
[Control of a SiC 2.5 MHz resonant full-bridge inverter for inductively driven plasma](#)  
2019. PCIM Europe 2019; International Exhibition and Conference for Power Electronics,  
Intelligent Motion, Renewable Energy and Energy Management, 1753–1760, VDE Verlag

Lizenzinformationen: [KITopen-Lizenz](#)